

Band Gap Opening in Bilayer Graphene-CrCl₃/CrBr₃/CrI₃ van der Waals Interfaces

Giulia Tenasini,^{1,2,*} David Soler-Delgado,^{1,2} Zhe Wang,^{1,3} Fengrui Yao,^{1,2} Dumitru Dumcenco,¹

Enrico Giannini,¹ Kenji Watanabe,⁴ Takashi Taniguchi,⁵ Christian Mouldsdales,^{6,7} Aitor

Garcia-Ruiz,^{6,7} Vladimir I. Fal'ko,^{6,7,8} Ignacio Gutiérrez-Lezama,^{1,2} and Alberto F. Morpurgo^{1,2,†}

¹Department of Quantum Matter Physics, University of Geneva, 24 Quai Ernest Ansermet, CH-1211 Geneva, Switzerland

²Group of Applied Physics, University of Geneva, 24 Quai Ernest Ansermet, CH-1211 Geneva, Switzerland

³MOE Key Laboratory for Non-equilibrium Synthesis and Modulation of Condensed Matter, Shaanxi Province Key Laboratory of Advanced Materials and Mesoscopic Physics, School of Physics, Xi'an Jiaotong University, Xi'an 710049, China.

⁴Research Center for Functional Materials, NIMS, 1-1 Namiki, Tsukuba 305-0044, Japan

⁵International Center for Materials Nanoarchitectonics, NIMS, 1-1 Namiki, Tsukuba 305-0044, Japan

⁶National Graphene Institute, University of Manchester, Manchester M13 9PL, UK

⁷School of Physics & Astronomy, University of Manchester, Manchester M13 9PL, UK

⁸Henry Royce Institute for Advanced Materials, Manchester M13 9PL, UK

(Dated: August 25, 2022)

We report experimental investigations of transport through bilayer graphene (BLG)/chromium trihalide (CrX₃; X=Cl, Br, I) van der Waals interfaces. In all cases, a large charge transfer from BLG to CrX₃ takes place (reaching densities in excess of 10^{13} cm⁻²), and generates an electric field perpendicular to the interface that opens a band gap in BLG. We determine the gap from the activation energy of the conductivity and find excellent agreement with the latest theory accounting for the contribution of the σ bands to the BLG dielectric susceptibility. We further show that for BLG/CrCl₃ and BLG/CrBr₃ the band gap can be extracted from the gate voltage dependence of the low-temperature conductivity, and use this finding to refine the gap dependence on the magnetic field. Our results allow a quantitative comparison of the electronic properties of BLG with theoretical predictions and indicate that electrons occupying the CrX₃ conduction band are correlated.

Van der Waals (vdW) interfaces provide a vast playground for creating new systems with engineered electronic properties, by stacking suitably chosen atomically thin crystals (or 2D materials) on top of each other. Examples include hexagonal Boron Nitride (hBN) encapsulation of graphene [1–3], proximity induced spin-orbit coupling in graphene on semiconducting transition metal dichalcogenide substrates [4–10], or the creation of so-called Γ – Γ interfaces [11, 12]. Recently, the discovery of 2D magnets and their use in vdW heterostructures has further broadened the scope of phenomena that can be explored [13–18]. In these systems, the wave functions of electrons in the non-magnetic material extend into the magnetic one and experience some of the magnetic interaction, enabling magnetism to be proximity induced in graphene or other 2D materials [13, 19–28]. However, deterministically controlling magnetism by proximity and predicting what aspect of magnetism can be induced into non-magnetic materials are challenges that remain to be solved because many different phenomena – such as strain, hybridization, charge transfer, and more – occur simultaneously at van der Waals interfaces [15, 29–31], influencing the interfacial electronic properties. In particular, electrostatic effects often dominate the behavior of heterostructures formed by low-charge-density systems, such as 2D semiconductors and semimetals. As a result, significant charge transfer can occur and lead to new phenomena mediated by changes in elec-

tron concentration or orbital occupation [32]. Indeed, recent work reported spin-dependent interlayer charge transfer in magnetic vdW heterostructures [33–35] and concluded that its detailed analysis is of key importance for improving the control of interfacial properties.

Here, we report the systematic behavior of vdW interfaces formed by bilayer graphene (BLG) [36, 37] and chromium trihalide crystals (CrX₃; X=Cl, Br, I) [38–45]. All systems exhibit a large transfer of electrons from graphene to the magnetic material, reaching values in excess of 10^{13} cm⁻², producing a large electric field perpendicular to the interface and a gap in BLG. When gating the BLG at the charge neutrality point (CNP), the gap induces a low-temperature suppression of the conductance of four orders of magnitude or more, exhibiting a sharp onset as a function of gate voltage. We determine the size of the band gap by analyzing the temperature dependence of the transfer curves (i.e., conductance-vs-gate voltage), and find excellent agreement with the results of the latest ab initio calculations of the electrostatically induced gap in BLG, which include dielectric screening due to the polarizability of the σ bonds in the graphene lattice [46]. We also find that the gap in BLG can be determined by looking exclusively at the low-temperature gate voltage dependence of the conductance, a result that provides information about the nature of the electronic states in the CrX₃, and that enables the quantitative determination of the dependence of the BLG band gap on the applied magnetic field.

* giulia.tenasini@unige.ch

† alberto.morpurgo@unige.ch

Figure 1a shows an optical microscope image of a

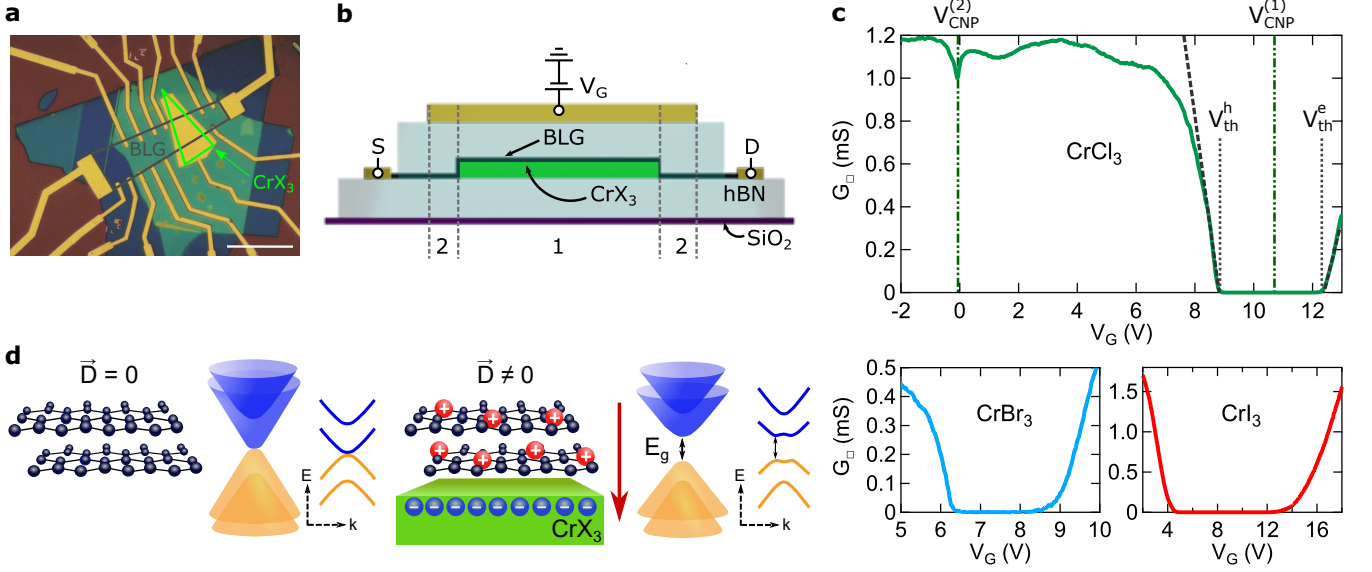


FIG. 1. Band gap opening in BLG/CrX₃ interfaces. (a) Optical micrograph and (b) schematics of a representative device (the scale bar in (a) is 20 μm), based on a BLG/CrX₃ heterostructure encapsulated in hBN. A metallic gate electrode is deposited onto the top hBN layer, and is coupled to two distinct regions: a central part formed by the BLG/CrX₃ interface (region 1) and two adjacent parts where BLG is in contact only with hBN (region 2). Transport is measured using metallic source (S) and drain contacts (D) and probes the two regions connected in series. (c) Square conductance G_{\square} as a function of gate voltage V_G measured in a heterostructure of BLG-on-CrCl₃ at 250 mK (green curve, top). Two characteristic features are visible in the transfer curve: a small conductance dip close to $V_G = 0$ V corresponding to the CNP of graphene in region 2 ($V_{CNP}^{(2)}$) and a pronounced suppression at large V_G ($V_{CNP}^{(1)}$) that originates from gating BLG-on-CrCl₃ (i.e., region 1) to charge neutrality. The black dashed lines represent linear extrapolations to extract the threshold voltages for holes V_{th}^h and electrons V_{th}^e . Virtually identical behaviour is observed in heterostructures of BLG and CrBr₃ (light-blue, bottom) and BLG-on-CrI₃ (red, bottom). (d) Schematics of the BLG band structure in the absence (left) and presence (right) of a perpendicular displacement field \vec{D} , showing that at finite field a gap E_g is present at charge neutrality. As visible on the right side of the panel, the displacement field is generated by the large transfer of electrons from BLG to CrX₃ occurring at the vdW interface.

representative device employed for our transport studies. A BLG with an elongated rectangular shape is placed on top of an exfoliated CrX₃ thin crystal, using a by-now conventional dry transfer method [47]. The process is carried out in the controlled environment of a glove box and the interface is encapsulated in hBN to prevent degradation upon exposure to air. Metal contacts to BLG are patterned using standard micro-fabrication techniques, and a gate electrode is deposited onto the top hBN, enabling the charge density in the BLG layer to be tuned. The device schematics in Figure 1b highlights how the gate is coupled to two distinct regions: a central part formed by the BLG/CrX₃ interface (which we refer to as region 1) and two parts on the sides, where BLG is in contact only with hBN (which we refer to as region 2) that effectively act as contacts to the gapped part of the structure. This device feature is important to understand some aspects of the measurements that we present later.

The gate voltage dependence of the square conductance G_{\square} of a device with BLG-on-CrCl₃, shown in Figure 1c (green curve), reveals two characteristic features that originate from regions 1 and 2. The small

conductance dip close to $V_G = 0$ V is the manifestation of the charge neutrality point (CNP) of BLG-on-hBN (region 2), and the pronounced suppression (four orders of magnitude) at large V_G originates from having gated BLG-on-CrCl₃ (region 1) to charge neutrality. The shift of the BLG CNP toward high, positive gate voltages indicates that a large number of electrons are transferred from BLG to the CrCl₃ crystal (10^{13} cm⁻²). Analogous behavior and a large hole doping in BLG (see Section S1 of the Supporting Information for transfer curves in a broader range of gate voltages) are also observed in heterostructures formed by BLG and CrBr₃ (light-blue curve) and in BLG-on-CrI₃ (red curve; in agreement with the earlier observations [32, 48]).

The observed charge transfer generates a strong electric field perpendicular to the interface that causes the opening of a band gap in BLG [37, 49–54] (see the schematic band diagrams in Figure 1d). As a result, when the chemical potential in BLG is shifted to charge neutrality by applying a suitable gate voltage, this leads to a robust insulating state. The sharp onset of this insulating state as a function of V_G implies the absence of large electrostatic potential fluctuations at the

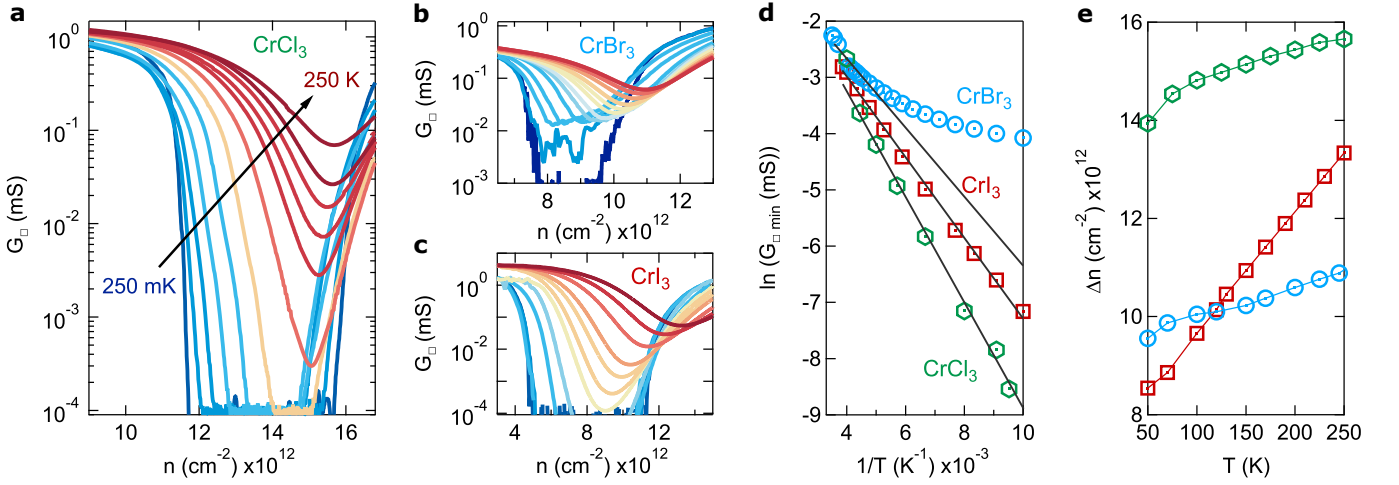


FIG. 2. **Temperature evolution of the square conductance in BLG/CrX₃ heterostructures.** Square conductance G_{\square} as function of charge density n measured at different temperatures between 250 mK (blue) and 250 K (red) for (a) BLG-on-CrCl₃, (b) CrBr₃ and (c) CrI₃. (d) Arrhenius plot of the minimum square conductance measured for the three different heterostructures (CrCl₃ green hexagons, CrI₃ red squares, CrBr₃ light-blue circles). Activation energies are obtained by fitting the linear part in the high-temperature range (grey lines). (e) Temperature dependence of the charge Δn transferred from BLG to CrX₃ for the investigated interfaces (the different colors and symbols represent data measured on different interfaces, as indicated in (d)).

BLG/CrX₃ interfaces, indicating that charge transfer from CrX₃ to BLG is rather homogeneous. To compare quantitatively the experimental observations made in heterostructures based on the different CrX₃, we convert the applied gate voltage to the corresponding accumulated charge density n , as $n = \frac{\epsilon \epsilon_0}{t} \frac{V_G - V_{\text{CNP}}^{(2)}}{e}$ (ϵ and t are the relative dielectric constant and thickness of the hBN layer, and $V_{\text{CNP}}^{(2)}$ is the gate voltage corresponding to the CNP in region 2, see Figure 1c). The concentration of electrons transferred from BLG in CrX₃ is then given by $\Delta n = \frac{\epsilon \epsilon_0}{t} \frac{V_{\text{CNP}}^{(1)} - V_{\text{CNP}}^{(2)}}{e}$ (where $V_{\text{CNP}}^{(1)}$ is the gate voltage corresponding to the CNP of BLG-on-CrX₃, i.e. in region 1; see Figure 1c again), and is directly proportional to the displacement field present at the BLG/CrX₃ interfaces, $D = e\Delta n$ (we use this relation to calculate the values of the displacement field in Figure 3).

We determine the size of the band gap from the temperature (T) evolution of the transfer curves, plotted in Figure 2a-c for CrCl₃, CrBr₃, and CrI₃, respectively. Data are shown for selected values of T between 250 mK (blue curve) and 250 K (red). The activation energies for the three heterostructures are extracted by looking at the minimum square conductance G_{\square}^{min} (corresponding to G_{\square} at the CNP of BLG/CrX₃), by fitting the linear part of the Arrhenius plot in the high-temperature range, where the charge carriers are dominated by a thermally activated behavior (see Figure 2d). The larger activation energy E_a is observed in BLG-on-CrCl₃ (green hexagons) where the gap ($E_g = 2E_a$) is estimated to be 162 meV; band gaps of 124 meV and 108 meV are found for BLG-on-CrI₃ (red squares) and on CrBr₃

(light-blue circles), respectively.

The same measurements show that the position of the CNP, i.e., the density of charge transferred from BLG to CrX₃, is temperature-dependent (as summarized in Figure 2e), implying that the perpendicular electric field responsible for the opening of the band is not constant as T is varied. For BLG-on-CrCl₃ (green) and on CrBr₃ (light-blue) the position of CNP changes by less than 10% throughout the full range investigated, and by significantly less over the range used to determine the size of the band gap, so that the effect can be disregarded. For CrI₃ (red) the change is larger, corresponding to a more sizable indetermination for the electric field value responsible for the opening of the gap in BLG. The precise microscopic origin of the T dependence of CNP in BLG-on-CrI₃ is currently not understood, and is likely determined by the electronic properties of CrX₃, which are materials with very narrow bands, whose behavior deviates from that of conventional semiconductors (see also the below discussion on the determination of the gap from the gate voltage dependence of the transfer curves).

The band gap dependence on the electric field for the three different BLG/CrX₃ interfaces is compared to the calculated gap in Figure 3. The electric field dependence of the gap predicted for $\epsilon_z = 2.6$ —corresponding to the theoretically expected dielectric susceptibility when accounting for the polarizability of the σ bands—is represented by the blue line. For comparison we also show calculations with $\epsilon_z = 1$ (grey line) as in [37]. The

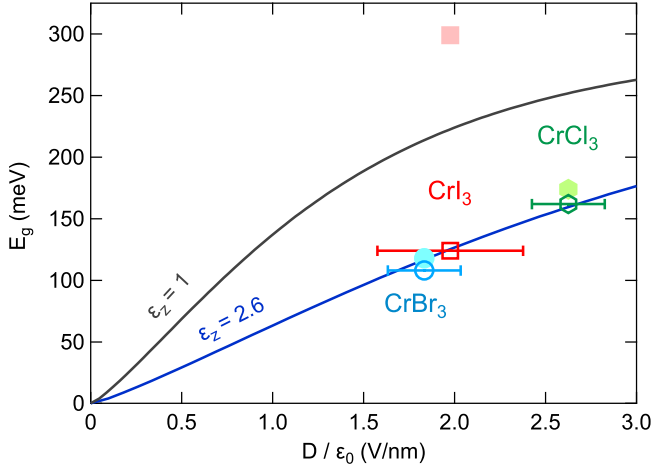


FIG. 3. **Electric field dependence of the band gap in BLG/CrX₃ interfaces.** The continuous lines represent the band gap as a function of displacement field D predicted by ab initio calculations, considering or ignoring the contribution to the dielectric susceptibility ϵ_z due to the electrons that occupy the σ band of BLG [46]. The empty symbols represent the experimental data obtained from the temperature dependence of the conductance measured in our devices. It is apparent that the experimental data are in excellent agreement with theoretical prediction for $\epsilon_z = 2.6$. The error bars for the displacement field ($D = e\Delta n$, see main text) correspond to the variation of charge transferred from BLG to CrX₃ (and consequently of D) as temperature is varied. Filled symbols indicate the experimental values of E_g extracted from the threshold voltages of low-temperature transfer curves using Equation (1). For CrCl₃ and CrBr₃ the agreement with the gap values obtained from the temperature-dependent measurements is excellent.

empty symbols of different colors (CrCl₃, green hexagon; CrI₃, red square; CrBr₃, light-blue circle) represent our experimental data, and the error bar denotes the indetermination on the electric field due to the temperature dependence of the charge transferred from BLG to CrX₃, as just discussed above. These data agree perfectly with theory that considers $\epsilon_z = 2.6$ using the method proposed in [46], and deviate very significantly from the $\epsilon_z = 1$ curve. This result should be underscored, because experimental values for the band gap reported in the early days of research on graphene were larger, and it was argued that quantitative agreement was obtained for $\epsilon_z = 1$ (the deviation likely originated from an insufficiently sharp dependence of the conductance on V_G due to the lower quality of the BLG-on-SiO₂ devices used in earlier experiments [54]).

Having determined the band gap from the analysis of the temperature dependence of the square conductance, we now present an alternative way that relies exclusively on the analysis of the low-temperature G_{\square} -vs- V_G curves. From analyzing our data, we find that for BLG on both

CrCl₃ and CrBr₃, the gap is quantitatively given by

$$E_g = \frac{C (V_{th}^e - V_{th}^h)}{e \rho_{BLG}} \quad (1)$$

Here, V_{th}^e and V_{th}^h are the threshold voltages for electron and hole conductance (obtained by extrapolating to zero the conductance measured as a function of gate voltage, as illustrated by the dashed lines in Figure 1c) and $\rho_{BLG} = 2m^*/\pi\hbar^2$ is the density of states in gapless BLG contacts (i.e., region 2 in Figure 1b), next to the gapped region where BLG is on the CrX₃ layer (region 1). Equation (1) gives the gap values represented with filled symbols in Figure 3, in perfect agreement with the values obtained from the T dependence of the minimum conductance for both BLG-on-CrCl₃ and BLG-on-CrBr₃; for BLG-on-CrI₃, instead, Eq. (1) gives a value that deviates by nearly a factor of 2 from the correct one. We discuss below the origin of Eq. (1), the condition for its validity, and why it fails to give the correct value of the gap for CrI₃.

The possibility to use Eq. (1) to extract the band gap of BLG enables the detailed dependence of the gap on the magnetic field, not yet addressed in previous studies, to be probed in an experimentally straightforward way. To this end, it suffices to measure the conductance as a function of gate voltage for different values of the magnetic field, as shown in Figure 4a for a BLG-on-CrCl₃ device. The left and right panels zoom in on the onset of threshold for both electron and hole conduction, which shift upon increasing the applied magnetic field, resulting in a decrease in $(V_{th}^e - V_{th}^h)$, and therefore a decrease in the BLG band gap. The full dependence of the gap on B for BLG-on-CrCl₃ and for BLG-on-CrBr₃ (represented by the green hexagons and light-blue circles, respectively) is compared to the theoretically calculated dependence (orange line) in Figure 4b. Theory predicts that the gap decreases as a result of the formation of Landau levels [1], which causes the top of the valence band to increase in energy and the bottom of the conduction band to decrease (see Figure 4c). This is a counter-intuitive behavior that contrasts what would be expected for electrons in a conventional two-dimensional electron gas (i.e., electrons described by a scalar wave function, for which the formation of Landau levels would lead to an increase in the gap at finite B). At a quantitative level, a change in the gap between 10% and 15% is expected as B increases up to 13 T, which results in perfect agreement with experiments without the need to introduce any free fitting parameters. To confirm the soundness of this result and exclude significant contributions of other mechanisms to the observed magnetic field dependence of the band gap, we also considered whether the charge transferred from BLG to CrX₃ depends on the magnetic field. This is important because a change in charge transfer would lead to a corresponding change in the perpendicular electric field and thus in the size of the band

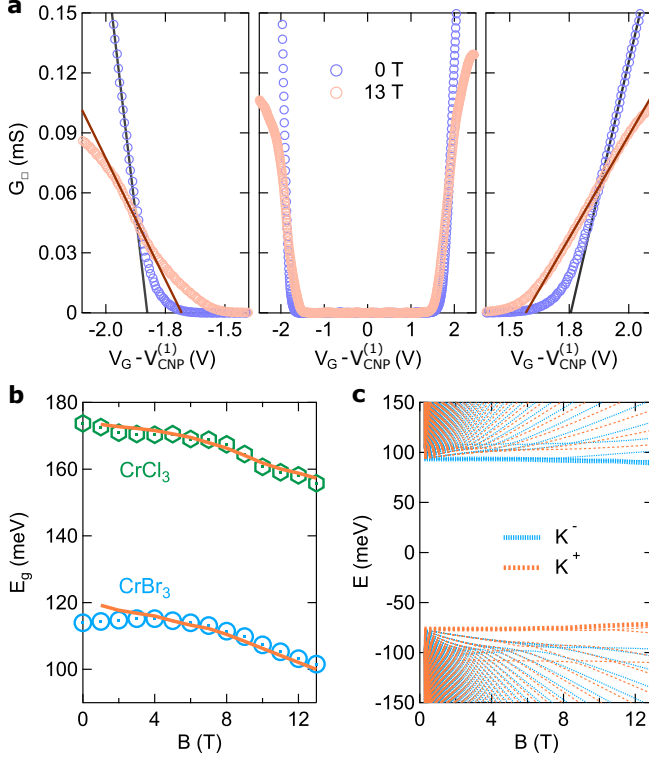


FIG. 4. Magnetic field dependence of the BLG band gap. (a), Square conductance G_{\square} as a function of gate voltage V_G shifted with respect to the value of CNP $V_{CNP}^{(1)}$, measured in a BLG/CrCl₃ heterostructure at 0 T and with an applied magnetic field of 13 T. The left and the right panels zoom in on the onset of conduction for holes and electrons: the corresponding threshold voltages V_{th}^h and V_{th}^e shift upon increasing the magnetic field, resulting in a decrease in $(V_{th}^e - V_{th}^h)$ and therefore in a decrease in the band gap extracted using Eq. (1). (b), Magnetic field dependence of the energy gap for BLG-on-CrCl₃ (green empty hexagons) and for BLG-on-CrBr₃ (light-blue empty circles); the size of the symbols corresponds to the experimental uncertainty associated with the error in the determination of the threshold voltages. The continuous orange lines represent the calculated band gap considering appropriate screened interlayer asymmetry potentials and including a screening potential for non-zero magnetic fields, as predicted by theory to calculate the Landau level spectrum. The experimental data are in excellent agreement with the theoretical predictions. (c), Landau levels calculated for a screened interlayer asymmetry potential of $|\Delta| = 215$ meV resulting in an experimentally observed gap of $E_g = 170$ meV at zero applied magnetic field. The dependence of the gap on the magnetic field is determined by the difference in the energies of the lowest Landau level in the conduction and valence bands.

gap. Nevertheless, the analysis of the magnetic field dependence of the CNP (Section S2 of the Supporting Information) shows that, even if charge transfer slightly decreases at high magnetic fields, the quantitative effect on the gap is very small, close to the sensitivity of the experiment, and negligible in a first approximation.

Such excellent quantitative agreement shows the usefulness of Eq. (1) and confirms its validity. To understand heuristically the origin of Eq. (1) we look at how the electrostatic and electrochemical potentials vary in the different regions of our devices (see Figure 1b), i.e., in region 1 where BLG is in contact with the CrX₃ layer and in region 2 where BLG is on hBN. A change ΔV_G in applied gate voltage causes a variation in the electrochemical and electrostatic potentials $\Delta\mu$ and $\Delta\phi$ in both regions, with the two quantities related by $\Delta\mu = e\Delta\phi + \Delta E_F$ (ΔE_F is the change in Fermi energy induced by the variation in the density of accumulated electrons in BLG, i.e., $\Delta E_F = C\Delta V_G / e\rho_{BLG}$). Since the entire structure is at equilibrium for all gate voltages, the change in electrochemical potential is uniform, such that $\Delta\mu^{(1)} = \Delta\mu^{(2)}$, or $e\Delta\phi^{(1)} + \Delta E_F^{(1)} = e\Delta\phi^{(2)} + \Delta E_F^{(2)}$. Whenever the electrochemical potential in region 1 is inside the gap of BLG –and at sufficiently low temperature– $\Delta E_F^{(1)} = 0$, because no states are available to add charge. Under these conditions, therefore, a variation in gate voltage only changes the electrostatic potential in region 1, so that we have $e\Delta\phi^{(2)} + \Delta E_F^{(2)} = e\Delta\phi^{(1)}$. As $\Delta E_F^{(2)} = C\Delta V_G / e\rho_{BLG}$, we obtain $e\Delta\phi^{(1)} - e\Delta\phi^{(2)} = C\Delta V_G / e\rho_{BLG}$, a relation that determines the relative band alignment between region 1 and 2. While we sweep the gate voltage from $V_G = V_{th}^h$ to $V_G = V_{th}^e$, this relation always holds, because throughout this V_G interval the electrochemical potential in region 1 is inside the gap. Since at $V_G = V_{th}^h$ the electrochemical potential in region 2 is aligned with the valence band edge in region 1 and at $V_G = V_{th}^e$ the electrochemical potential in region 2 is aligned with the conduction band edge in region 1, we obtain $E_g = e\Delta\phi^{(1)} - e\Delta\phi^{(2)}$, and Eq. (1) then follows directly using that $e\Delta\phi^{(1)} - e\Delta\phi^{(2)} = C\Delta V_G / e\rho_{BLG}$. We interpret this result by saying that a change in V_G lowers the bands of BLG in region 1 and in region 2 (which effectively forms the source and drain contacts to the transistor channel), but changes E_F only in region 2 (because only region 2 is gapless), and it is this change in Fermi energy that shifts the electrochemical potential from the valence to the conduction band edge.

The argument above relies on the assumption that charge transferred from BLG to the underlying CrX₃ layer is fixed: at low temperature, a change in V_G does not change the charge accumulated in the CrX₃ layer. This is not what would happen if electrons in CrX₃ behaved as independent, non-interacting particles, i.e., if CrX₃ could be described as a conventional semiconductor. We attribute this behavior to the very narrow bands of CrX₃ –electrons added to CrX₃ are virtually localized on the Cr orbitals– which make electrons hosted in these materials strongly correlated, because the strength of their Coulomb interaction is larger than the bandwidth. As a result, at low temperature, the electrons transferred from BLG to the surface of CrX₃ create an energetically

stable correlated state (we imagine a spatially ordered distribution of electrons localized on Cr atoms that minimizes energy), which has an energy gap for adding or removing electrons. This assumption appears to be fully consistent with the behavior observed in BLG interfaces with CrCl_3 and CrBr_3 , for which Eq. (1) works perfectly, but not for BLG-on- CrI_3 , for which Eq. (1) gives a factor of 2 deviation as compared to the actual gap. The reason for this difference between the different CrX_3 compounds likely originates from the fact that the charge transferred from BLG to CrI_3 does vary as V_G is varied (possibly because the width of the conduction band of CrI_3 is somewhat larger than that of CrCl_3 and CrBr_3), an observation that seems consistent with the pronounced temperature dependence of charge transfer from BLG to CrI_3 (see Figure 2e). This conclusion underscores the unconventional nature of the semiconducting properties of chromium trihalides, which calls for more detailed future investigations, and the fact that the study of transport through BLG/ CrX_3 interfaces allows differences in the electronic properties of the different members of this family to be evidenced.

In summary, we have performed a systematic analysis of different phenomena determining the transport properties of vdW interfaces based on BLG and chromium trihalide crystals (CrCl_3 , CrBr_3 and CrI_3). In all cases, a very large charge transfer from graphene to CrX_3 is found to occur, which causes the opening of a band gap in BLG. A detailed comparison shows that the values of the gap determined experimentally are in excellent agreement with the latest ab initio calculations, which include the effect of the polarizability of the σ bands in the graphene honeycomb lattice. We furthermore show that it is possible to determine the band gap quantitatively by looking exclusively at the low-temperature gate voltage dependence of the conductivity, a finding that we exploit to determine how the band gap depends on the applied magnetic field. Besides providing indications as to the correlated nature of electrons transferred onto

the very narrow conduction band of CrX_3 , our work establishes a remarkable quantitative agreement between different electronic properties of BLG and corresponding theoretical predictions.

SUPPORTING INFORMATION

The Supporting Information is available free of charge on the ACS publications website at <https://pubs.acs.org/doi/10.1021/acs.nanolett.2c02369>.

- Transfer curves for BLG-on- CrBr_3 and BLG-on- CrI_3 devices; Magnetic field dependence of charge neutrality point.

ACKNOWLEDGEMENTS

The authors gratefully acknowledge Alexandre Ferreira for technical support, and Nicolas Ubrig and Sergey Slizovskiy for fruitful discussions. We acknowledge support from the Swiss National Science Foundation, the EU Graphene Flagship project, EPSRC CDT Graphene-NOWNANO, and EPSRC grants EP/S030719/1 and EP/V007033/1. Z. W. acknowledges the National Natural Science Foundation of China (Grants no. 11904276) and the Fundamental Research Funds for the Central Universities. K. W. and T. T. acknowledge support from the Elemental Strategy Initiative conducted by the MEXT, Japan (Grant Number JPMXP0112101001) and JSPS KAKENHI (Grant Numbers 19H05790, 20H00354, and 21H05233).

NOTES

G.T. and D.S.D. contributed equally to this work. The authors declare no competing financial interest.

-
- [1] A. Varlet, D. Bischoff, P. Simonet, K. Watanabe, T. Taniguchi, T. Ihn, K. Ensslin, M. Mucha-Kruczyński, and V. I. Fal’ko, Anomalous sequence of quantum hall liquids revealing a tunable lifshitz transition in bilayer graphene, *Physical Review Letter* **113**, 116602 (2014).
 - [2] R. Ribeiro-Palau, C. Zhang, K. Watanabe, T. Taniguchi, J. Hone, and C. R. Dean, Twistable electronics with dynamically rotatable heterostructures, *Science* **361**, 690 (2018).
 - [3] N. R. Finney, M. Yankowitz, L. Muraleetharan, K. Watanabe, T. Taniguchi, C. R. Dean, and J. Hone, Tunable crystal symmetry in graphene–boron nitride heterostructures with coexisting moiré superlattices, *Nature Nanotechnology* **14**, 1029 (2019).
 - [4] A. Avsar, J. Y. Tan, T. Taychatanapat, J. Balakrishnan, G. K. Koon, Y. Yeo, J. Lahiri, A. Carvalho, A. S. Rodin, E. C. O’Farrell, G. Eda, A. H. C. Neto, and B. Özyilmaz, Spin–orbit proximity effect in graphene, *Nature Communications* **5**, 4875 (2014).
 - [5] Z. Wang, D. Ki, H. Chen, H. Berger, A. H. MacDonald, and A. F. Morpurgo, Strong interface-induced spin–orbit interaction in graphene on WS_2 , *Nature Communications* **6**, 8339 (2015).
 - [6] Z. Wang, D.-K. Ki, J. Y. Khoo, D. Mauro, H. Berger, L. S. Levitov, and A. F. Morpurgo, Origin and Magnitude of ‘Designer’ Spin-Orbit Interaction in Graphene on Semiconducting Transition Metal Dichalcogenides, *Physical Review X* **6**, 041020 (2016).
 - [7] M. Gmitra and J. Fabian, Proximity Effects in Bilayer Graphene on Monolayer WSe_2 : Field-Effect Spin Valley Locking, Spin-Orbit Valve, and Spin Transistor, *Physical Review Letter* **119**, 146401 (2017).

- [8] T. S. Ghiasi, J. Ingla-Aynés, A. A. Kaverzin, and B. J. van Wees, Large Proximity-Induced Spin Lifetime Anisotropy in Transition-Metal Dichalcogenide/Graphene Heterostructures, *Nano Letters* **17**, 7528 (2017).
- [9] J. Y. Khoo, A. F. Morpurgo, and L. Levitov, On-demand spin-orbit interaction from which-layer tunability in bilayer graphene, *Nano Letters* **17**, 7003 (2017).
- [10] L. A. Benítez, J. F. Sierra, W. Saverio Torres, A. Arrighi, F. Bonell, M. V. Costache, and S. O. Valenzuela, Strongly anisotropic spin relaxation in graphene-transition metal dichalcogenide heterostructures at room temperature, *Nature Physics* **14**, 303 (2018).
- [11] D. J. Terry, V. Zólyomi, M. Hamer, A. V. Tyurnina, D. G. Hopkinson, A. M. Rakowski, S. J. Magorrian, N. Clark, Y. M. Andreev, O. Kazakova, K. Novoselov, S. J. Haigh, V. I. Fal'ko, and R. Gorbachev, Infrared-to-violet tunable optical activity in atomic films of GaSe, InSe, and their heterostructures, *2D Materials* **5**, 041009 (2018).
- [12] N. Ubrig, E. Ponomarev, J. Zultak, D. Domaretskiy, V. Zólyomi, D. Terry, J. Howarth, I. Gutiérrez-Lezama, A. Zhukov, Z. R. Kudrynskiy, Z. D. Kovalyuk, A. Patané, T. Taniguchi, K. Watanabe, R. V. Gorbachev, V. I. Fal'ko, and A. F. Morpurgo, Design of van der Waals interfaces for broad-spectrum optoelectronics, *Nature Materials* **19**, 299 (2020).
- [13] D. Zhong, K. L. Seyler, X. Linpeng, R. Cheng, N. Sivadas, B. Huang, E. Schmidgall, T. Taniguchi, K. Watanabe, M. A. McGuire, W. Yao, D. Xiao, K.-M. C. Fu, and X. Xu, Van der Waals engineering of ferromagnetic semiconductor heterostructures for spin and valleytronics, *Science Advances* **3**, e1603113 (2017).
- [14] M. Gibertini, M. Koperski, A. F. Morpurgo, and K. S. Novoselov, Magnetic 2D materials and heterostructures, *Nature Nanotechnology* **14**, 408 (2019).
- [15] C. Gong and X. Zhang, Two-dimensional magnetic crystals and emergent heterostructure devices, *Science* **363**, eaav4450 (2019).
- [16] K. F. Mak, J. Shan, and D. C. Ralph, Probing and controlling magnetic states in 2D layered magnetic materials, *Nature Reviews Physics* **1**, 646 (2019).
- [17] B. Huang, M. A. McGuire, A. F. May, D. Xiao, P. Jarillo-Herrero, and X. Xu, Emergent phenomena and proximity effects in two-dimensional magnets and heterostructures, *Nature Materials* **19**, 1276 (2020).
- [18] H. Kurebayashi, J. H. Garcia, S. Khan, J. Sinova, and S. Roche, Magnetism, symmetry and spin transport in van der Waals layered systems, *Nature Reviews Physics* **4**, 150 (2022).
- [19] Z. Qiao, W. Ren, H. Chen, L. Bellaiche, Z. Zhang, A. H. MacDonald, and Q. Niu, Quantum anomalous hall effect in graphene proximity coupled to an antiferromagnetic insulator, *Physical Review Letter* **112**, 116404 (2014).
- [20] J. C. Leutenantsmeyer, A. A. Kaverzin, M. Wojtaszek, and B. J. V. Wees, Proximity induced room temperature ferromagnetism in graphene probed with spin currents, *2D Materials* **4**, 014001 (2016).
- [21] C. Tang, B. Cheng, M. Aldosary, Z. Wang, Z. Jiang, K. Watanabe, T. Taniguchi, M. Bockrath, and J. Shi, Approaching quantum anomalous Hall effect in proximity-coupled YIG/graphene/h-BN sandwich structure, *APL Materials* **6**, 026401 (2017).
- [22] K. L. Seyler, D. Zhong, B. Huang, X. Linpeng, N. P. Wilson, T. Taniguchi, K. Watanabe, W. Yao, D. Xiao, M. A. McGuire, K. M. C. Fu, and X. Xu, Valley Manipulation by Optically Tuning the Magnetic Proximity Effect in WSe₂/CrI₃ Heterostructures, *Nano Letters* **18**, 3823 (2018).
- [23] C. Cardoso, D. Soriano, N. A. García-Martínez, and J. Fernández-Rossier, Van der Waals spin valves, *Physical Review Letter* **121**, 067701 (2018).
- [24] M. U. Farooq and J. Hong, Switchable valley splitting by external electric field effect in graphene/CrI₃ heterostructures, *npj 2D Materials and Applications* **3**, 1 (2019).
- [25] C. Tang, Z. Zhang, S. Lai, Q. Tan, and W. Gao, Magnetic Proximity Effect in Graphene/CrBr₃ van der Waals Heterostructures, *Advanced Materials* **32**, 1908498 (2020).
- [26] Y. Wu, Q. Cui, M. Zhu, X. Liu, Y. Wang, J. Zhang, X. Zheng, J. Shen, P. Cui, H. Yang, and S. Wang, Magnetic Exchange Field Modulation of Quantum Hall Ferromagnetism in 2D van der Waals CrCl₃/Graphene Heterostructures, *ACS Applied Materials and Interfaces* **13**, 10656 (2021).
- [27] M. Vila, J. H. Garcia, and S. Roche, Valley-polarized quantum anomalous hall phase in bilayer graphene with layer-dependent proximity effects, *Physical Review B* **104**, L161113 (2021).
- [28] T. S. Ghiasi, A. A. Kaverzin, A. H. Dismukes, D. K. de Wal, X. Roy, and B. J. van Wees, Electrical and thermal generation of spin currents by magnetic bilayer graphene, *Nature Nanotechnology* **16**, 788 (2021).
- [29] M. M. Ugeda, A. J. Bradley, S. F. Shi, F. H. D. Jornada, Y. Zhang, D. Y. Qiu, W. Ruan, S. K. Mo, Z. Hussain, Z. X. Shen, F. Wang, S. G. Louie, and M. F. Crommie, Giant bandgap renormalization and excitonic effects in a monolayer transition metal dichalcogenide semiconductor, *Nature Materials* **13**, 1091 (2014).
- [30] Q. Tong, M. Chen, and W. Yao, Magnetic Proximity Effect in a van der Waals Moiré Superlattice, *Physical Review Applied* **12**, 024031 (2019).
- [31] B. Zhou, J. Balgley, P. Lampen-Kelley, J. Q. Yan, D. G. Mandrus, and E. A. Henriksen, Evidence for charge transfer and proximate magnetism in graphene- α -RuCl₃ heterostructures, *Physical Review B* **100**, 165426 (2019).
- [32] S. Jiang, L. Li, Z. Wang, K. F. Mak, and J. Shan, Controlling magnetism in 2D CrI₃ by electrostatic doping, *Nature Nanotechnology* **13**, 549 (2018).
- [33] D. Zhong, K. L. Seyler, X. Linpeng, N. P. Wilson, T. Taniguchi, K. Watanabe, M. A. McGuire, K. M. C. Fu, D. Xiao, W. Yao, and X. Xu, Layer-resolved magnetic proximity effect in van der Waals heterostructures, *Nature Nanotechnology* **15**, 187 (2020).
- [34] T. P. Lyons, D. Gillard, A. Molina-Sánchez, A. Misra, F. Withers, P. S. Keatley, A. Kozikov, T. Taniguchi, K. Watanabe, K. S. Novoselov, J. Fernández-Rossier, and A. I. Tartakovskii, Interplay between spin proximity effect and charge-dependent exciton dynamics in MoSe₂/CrBr₃ van der Waals heterostructures, *Nature Communications* **11**, 1 (2020).
- [35] S. Mashhadi, Y. Kim, J. Kim, D. Weber, T. Taniguchi, K. Watanabe, N. Park, B. Lotsch, J. H. Smet, M. Burghard, and K. Kern, Spin-Split Band Hybridization in Graphene Proximitized with α -RuCl₃ Nanosheets, *Nano Letters* **19**, 4659 (2019).
- [36] K. S. Novoselov, E. McCann, S. V. Morozov, V. I. Fal'ko, M. I. Katsnelson, U. Zeitler, D. Jiang, F. Schedin, and

- A. K. Geim, Unconventional quantum Hall effect and Berry's phase of 2π in bilayer graphene, *Nature Physics* **2**, 177 (2006).
- [37] E. McCann and V. I. Fal'ko, Landau-Level Degeneracy and Quantum Hall Effect in a Graphite Bilayer, *Physical Review Letters* **96**, 086805 (2006).
- [38] H. Wang, V. Eyert, and U. Schwingenschlöggl, Electronic structure and magnetic ordering of the semiconducting chromium trihalides CrCl_3 , CrBr_3 , and CrI_3 , *Journal of Physics: Condensed Matter* **23**, 116003 (2011).
- [39] W.-B. Zhang, Q. Qu, P. Zhu, and C.-H. Lam, Robust intrinsic ferromagnetism and half semiconductivity in stable two-dimensional single-layer chromium trihalides, *J. Mater. Chem. C* **3**, 12457 (2015).
- [40] M. A. McGuire, H. Dixit, V. R. Cooper, and B. C. Sales, Coupling of crystal structure and magnetism in the layered, ferromagnetic insulator CrI_3 , *Chemistry of Materials* **27**, 612 (2015).
- [41] J. Liu, Q. Sun, Y. Kawazoe, and P. Jena, Exfoliating biocompatible ferromagnetic cr-trihalide monolayers, *Phys. Chem. Chem. Phys.* **18**, 8777 (2016).
- [42] B. Huang, G. Clark, E. Navarro-Moratalla, D. R. Klein, R. Cheng, K. L. Seyler, D. Zhong, E. Schmidgall, M. A. McGuire, D. H. Cobden, W. Yao, D. Xiao, P. Jarillo-Herrero, and X. Xu, Layer-dependent ferromagnetism in a van der Waals crystal down to the monolayer limit, *Nature* **546**, 270 (2017).
- [43] Z. Wang, I. Gutiérrez-Lezama, N. Ubrig, M. Kroner, M. Gibertini, T. Taniguchi, K. Watanabe, A. Imamoğlu, E. Giannini, and A. F. Morpurgo, Very large tunneling magnetoresistance in layered magnetic semiconductor CrI_3 , *Nature Communications* **9**, 1 (2018).
- [44] Z. Wang, M. Gibertini, D. Dumcenco, T. Taniguchi, K. Watanabe, E. Giannini, and A. F. Morpurgo, Determining the phase diagram of atomically thin layered antiferromagnet CrCl_3 , *Nature Nanotechnology* **14**, 1116 (2019).
- [45] S. Acharya, D. Pashov, B. Cunningham, A. N. Rudenko, M. Rösner, M. Grüning, M. van Schilfgaarde, and M. I. Katsnelson, Electronic structure of chromium trihalides beyond density functional theory, *Physical Review B* **104**, 155109 (2021).
- [46] S. Slizovskiy, A. Garcia-Ruiz, A. I. Berdyugin, N. Xin, T. Taniguchi, K. Watanabe, A. K. Geim, N. D. Drummond, and V. I. Fal'ko, Out-of-Plane Dielectric Susceptibility of Graphene in Twistrionic and Bernal Bilayers, *Nano Letters* **21**, 6678 (2021).
- [47] P. J. Zomer, S. P. Dash, N. Tombros, and B. J. van Wees, A transfer technique for high mobility graphene devices on commercially available hexagonal boron nitride, *Applied Physics Letters* **99**, 232104 (2011).
- [48] S. Jiang, L. Li, Z. Wang, J. Shan, and K. F. Mak, Spin tunnel field-effect transistors based on two-dimensional van der Waals heterostructures, *Nature Electronics* **2**, 159 (2019).
- [49] E. McCann, Asymmetry gap in the electronic band structure of bilayer graphene, *Physical Review B* **74**, 161403 (2006).
- [50] T. Ohta, A. Bostwick, T. Seyller, K. Horn, and E. Rotenberg, Controlling the electronic structure of bilayer graphene, *Science* **313**, 951 (2006).
- [51] E. V. Castro, K. S. Novoselov, S. V. Morozov, N. M. R. Peres, J. M. B. L. dos Santos, J. Nilsson, F. Guinea, A. K. Geim, and A. H. C. Neto, Biased bilayer graphene: Semiconductor with a gap tunable by the electric field effect, *Physical Review Letter* **99**, 216802 (2007).
- [52] J. B. Oostinga, H. B. Heersche, X. Liu, A. F. Morpurgo, and L. M. Vandersypen, Gate-induced insulating state in bilayer graphene devices, *Nature Materials* **7**, 151 (2008).
- [53] A. B. Kuzmenko, I. Crassee, D. van der Marel, P. Blake, and K. S. Novoselov, Determination of the gate-tunable band gap and tight-binding parameters in bilayer graphene using infrared spectroscopy, *Physical Review B* **80**, 165406 (2009).
- [54] Y. Zhang, T. T. Tang, C. Girit, Z. Hao, M. C. Martin, A. Zettl, M. F. Crommie, Y. R. Shen, and F. Wang, Direct observation of a widely tunable bandgap in bilayer graphene, *Nature* **459**, 820 (2009).